IEEE Access
Multidisciplinary | Rapid Review | Open Access Journal

Received 20 May 2024, accepted 4 June 2024, date of publication 12 June 2024, date of current version 20 June 2024.

Digital Object Identifier 10.1109/ACCESS.2024.3413153

RESEARCH ARTICLE

Unsteady Aerodynamics Over NACA0005 Airfoil for Ultra-Low Reynolds Numbers

TAIBA KOUSER[1], DILEK FUNDA KURTULUS[2], ABDULRAHMAN ALIYU[1], SRIKANTH GOLI[1], LUAI M. ALHEMS[1], IMIL HAMDA IMRAN[1], AND AZHAR M. MEMON[1]

[1]Applied Research Center for Metrology, Standards and Testing, King Fahd University of Petroleum and Minerals (KFUPM), Dhahran 31261, Saudi Arabia
[2]Aerospace Engineering Department, Middle East Technical University (METU), 06800 Ankara, Turkey

Corresponding author: Taiba Kouser (taiba.kouser@kfupm.edu.sa)

This work was supported in part by the King Fahd University of Petroleum and Minerals (KFUPM), and in part by the Applied Research Centre for Metrology Standards and Testing, KFUPM.

ABSTRACT In the present study, numerical simulation for a two-dimensional NACA0005 is performed for angles of attack $\alpha = 0° - 15°$. The Reynolds numbers 1000, 2000 and 5000 are considered. Simulations show that the flow fields can be classified due to characteristics of vortex shedding based on Reynolds number and angle of attack. Furthermore, this study reveals that in the case of thinner airfoils, several modes (Mode I, Mode II, Mode III) are present at the same angle of attack for varying Reynolds number. Maximum lift to drag ratio is found at Reynolds number 5000 and angle of attack 6° as well as gradual stall is observed. Onset of oscillations to determine critical angles of attack is reported for NACA0005 with the dominant frequencies. A subcategory of mode III termed as mode IIIa/c, and recently reported mode 4i is also observed in present study. A new mode termed as k-mode is discovered for higher angles of attack at Re = 5000. In addition, numerical simulations of two-dimensional periodic flows around NACA0005 profile at Reynolds number Re = 5000 demonstrate that unsteady periodic flows reach different saturation states at angles of attack of $10° - 15°$. The coexisting periodic states and period-doubling (with higher and lower intensities) in this range indicate that the wake undergoes substantial changes from the Von-Kármán vortex street.

INDEX TERMS Airfoil, critical angle, flow modes, k-mode, low reynolds number, NACA0005.

I. INTRODUCTION

The low Reynold number (Re) flows over foils have immense applications including naval engineering, energy harvesting, unmanned aerial vehicles (UAV). Many micro and mini UAVs operate at low speeds and altitudes, resulting in low Reynolds number flows over their wings. Understanding the aerodynamic performance of airfoils at low Reynolds numbers can contribute significantly to extract sustainable energy and energy conservation efforts by considering the aerodynamic force. Engineers and designers often aim to minimize the drag coefficient in various applications, from car design to the aerodynamics of aircraft, to enhance efficiency and speed. In marine equipment as well as aircraft, airfoils are widely used as lifting surfaces to balance gravity or buoyancy and to manipulate the motion of a vehicle. Micro-air vehicles (MAVs) and autonomous underwater vehicles (AUVs) are more and more often equipped with airfoils as they become smaller and more compact. Across all these vehicles, the rotating wings, or rotors, operate on small geometric scales, which results in ultra-low Reynolds number flow around the blades. Mars exploration UAVs have also received recent interest as fast and mobile alternatives to ground-based rovers. A Mars mission requires aerial vehicles with low Reynolds numbers aerodynamics because of the low atmosphere density and temperature on Mars [1], [2]. Laminar separation bubbles have been extensively studied as this characteristic contributes to the degradation in performance of airfoils at high Re [3], [4]. In the attached boundary layer on the surface of the airfoil, laminar separation bubbles are formed when the flow starts to be detached. Research on the low-Reynolds-number range $10^4 - 10^6$ has been

The associate editor coordinating the review of this manuscript and approving it for publication was Rosario Pecora.

focused on by most researchers [5], [6]. However, it excludes the Reynolds numbers less than 10^4 which is of particular interest to MAV, UAV, and low-speed flight designers. The low Reynolds number of this range is of great importance for the initial flight of these vehicles. Due to the importance of ultra-low Reynolds number in growing UAV industry, several researchers have focused on aerodynamic performance of airfoils for Reynolds number less than 10^4 [7], [8], [9], [10], [11], [12], [13].

The flow field in low Reynolds number regimes must be understood to operate MAVs properly. Furthermore, the physical interpretation and understanding of flapping airfoils' vortex formations can be improved by studying the unsteady flow field behind stationary airfoils with steady external conditions. At different angles of attack, instantaneous wake structures behind NACA0002 airfoil for $Re \in [100 - 3000]$ are numerically studied [7]. The performance of airfoil can adversely be affected by unsteady wake patterns at trailing edge [14]. Therefore, it is crucial to understand the lift and thrust forces generation mechanism at ultra-low Reynolds numbers to propose more efficient and better designs for small swimming and flying unmanned vehicles. Generation of the Von-Karman vortex stream and the separation from the trailing edge is observed for low angles of attack at $Re = 10^3$ [15]. Uddin et al. [16] investigated the three NACA four-digit symmetric airfoils with thicknesses of 8%, 12%, and 16% at Reynolds number 1000 demonstrated unsteady aerodynamic behavior.

The effect on lift hysteresis loop was documented by Huang et al. [17] and Bao et al. [18] by coupling the smoothed particle hydrodynamics and finite difference method. Predominant effect on lift hysteresis at lower and medium Reynolds numbers was observed for high velocity and pitching axis position. The numerical study of Pulliam and Vastano was based on increasing Reynolds numbers between 800 and 1,600 to investigate unsteady flows past NACA0012 [19]. A bifurcation sequence leading from a simple periodic flow to complex chaotic behavior was examined in order to understand the transition from stability to unsteadiness. It is observed that flow undergoes a period-doubling bifurcation leads to chaotic behavior for the increasing $Re \in$ [800-1600]. Similarly, symmetric NACA0010 airfoils exhibited similar behavior under similar flow conditions, as recently reported by Durante et al. [20].

Vortical structures are highly oscillatory at low Reynolds numbers as the viscosity of the fluid dampens the flow, causing vortices to shed and dissipate more quickly. The flow tends to be more laminar and orderly, with vortices forming and dissipating rapidly. Consequently, aerodynamic forces show high amplitude. The vortices shed in the wake are categorized in several modes as single mode (2S) or mode II for $8° \sim 15°$, chaotic state for $16° \sim 18°$, and quasi periodic flow for $20° \sim 24°$. Furthermore, the increase in angle of attack (AOA) has a negative impact on stability of flow field. As the angle of attack is increased, Strouhal number (St) decreases. The order of the St is higher for single periodic mode as compared to quasi periodic and chaotic flow states [21]. Rossi et al. [22] have pointed out that Reynolds-based bifurcations exist in the flow fields behind airfoils at low Reynolds numbers where the wake patterns bifurcate between different modes even at a constant angle of attack. Simulations are performed over Eppler-61 and NACA0009 airfoils to predict the flow characteristics for Reynolds numbers ranging 5000 - 60000 [23]. The investigation accounts three stages of angle-of-attack dependent transition, progressing from fully laminar to partially turbulent airflow around the airfoils. A stabilized laminar wake, well-ordered vortex street, and the formation of separation bubble were characterized in these three phases respectively. With an increasing angle of attack, the flow pattern changes phases; the exact angle at which the changes occur depends on the airfoil and Reynolds number. Although many parameters are involved, mechanisms are still not fully understood for generating unsteady forces [23].

Laminar or turbulent flow on airfoil surface is influenced by boundary-layer physics including flow separation, re-attachment zones, and laminar or turbulent flow separation. An unsteady aerodynamic investigation was conducted by Deng et al. [24] for a NACA0015 airfoil with Re from 100 to 1,300 for angles of attack ranging from $10° - 20°$. In order to investigate the wake behavior and near body flow, they investigated Strouhal number and Reynolds number correlations. Recently, several studies have been conducted for various 4-digit family of NACA for low Reynolds number [25], [26]. However, study on NACA0005 is missing for ultra-low Reynolds numbers. This study aims to investigate the effects of vortex shedding unsteadiness over NACA0005. Based on literature, the current study attempts to provide a deeper understanding of how flow around NACA0005 airfoil behaves at low Reynolds numbers ($Re = 1000$ to 5000), effect of angles of attack on flow patterns, and impact on the aerodynamic performance of NACA0005. The present investigation analyzes the flow around a NACA0005 airfoil with a thickness of 5% in a two-dimensional setup. The study covers angles of attack ranging from 0° to 15° for increasing Re. Furthermore, the results are compared in accordance with other airfoils of the family. At each angle of attack but different Reynolds number, different wake patterns identified by Kurtulus [14], Rossi et al. [22], and Durante et al. [20] are described along with a newly discovered pattern (k-mode). Studies are compared to evaluate the effect of airfoil thickness on the modes exhibited and the change in aerodynamic coefficients associated with mode transitions. Hence, in the present study, low Reynolds numbers are defined as chord-based Reynolds numbers between 1000-5000. This article is organized as follows: section II presents the computational domain and methodology used for simulation. Results and discussion are illustrated in sections III and IV. In section III, the instantaneous and mean behavior of aerodynamic coefficients as well as frequency analysis are reported. Whereas, in section IV, transitional wake flown patterns

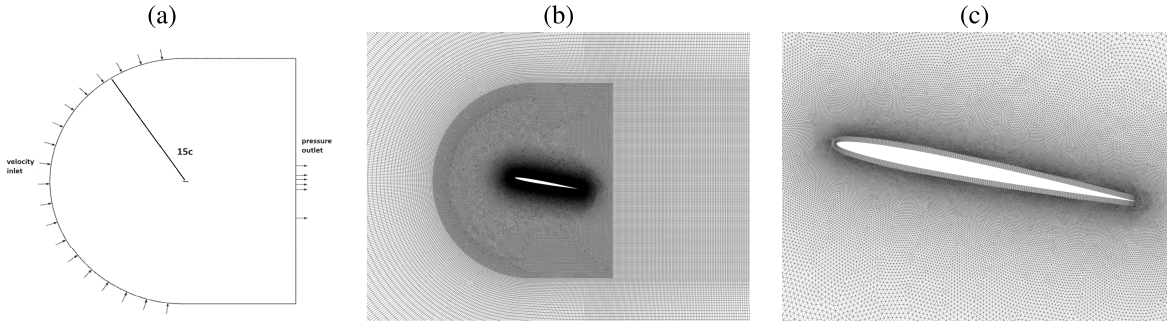

FIGURE 1. (a) Computational domain (b) subdomain adjacent to airfoil (c) mesh topology in the vicinity of NACA0005 profile at $\alpha = 5°$.

TABLE 1. Comparative results for laminar and turbulence models at $\alpha = 6°$, $\alpha = 10°$ and $\alpha = 15°$.

Re	Viscous models	$\bar{C}_l$	$\bar{C}_d$
$\alpha = 6^o$			
1000	Laminar	0.436	0.1174
5000	Laminar	0.637	0.0780
5000	SST 4-equations	0.638	0.0783
5000	$k-\omega$ SST	0.639	0.0786
$\alpha = 10^o$			
5000	Laminar	1.111	0.2139
5000	SST 4-equations	1.0375	0.1932
5000	$k-\omega$ SST	1.107	0.2145
$\alpha = 15^o$			
5000	Laminar	1.345	0.3942
5000	SST 4-equations	1.251	0.3693
5000	$k-\omega$SST	1.229	0.3462

are discussed. A short conclusion is provided in the last section V.

II. METHODOLOGY

A 4-digit symmetric low thickness airfoil NACA0005 is used to conduct the study. Laminar, incompressible, unsteady, and 2D Navier-Stokes equations along with turbulence models (k-omega SST) [27], [28], and SST 4-equations [29] are utilized for computational purposes. Simulations are carried out at Reynolds number ranging from 1000-5000 defined as $Re = \frac{\rho U c}{\mu}$, where ρ is the density of air, U represents the free-stream velocity, μ is dynamic viscosity of air and $c = 0.1$m is chord length of symmetric airfoil used (Fig. 1).

In order to form the grid domain, the symmetric airfoil is pivoted from the quarter chord location and rotated with the associated angle of attack. The same grid domain and meshing are used for numerical study as grid domain surrounding the airfoil consists of subdomains: One sub-domain adjacent to the airfoil and one outside the inner domain, extending $19c$ downstream and upstream (Fig. 1). As part of the preprocessor program, the airfoil is rotated according to the angle of attack for the inner domain while keeping the outer domain and wake regions fixed using the same grid structure. Figure 1 illustrates the diagram of the computational domain and the grid system. A zero-reference value is specified for the Neumann boundary condition and gauge pressure at the outlet. Current results are obtained by using a two-dimensional finite volume solver (ANSYS Fluent v22.0). An implicit SIMPLE algorithm is used, coupled with gauge pressure and velocity to obtain second order solutions in time and space. A medium mesh configuration with elements in the order of $2 * 10^5$ has a first spacing of 0.002c for the boundary layer. The medium mesh configuration has 300 nodes around the airfoil (Fig. 1). Detailed mesh and time refinement studies have been performed in previous work [30]. Similarly, the medium mesh size and time increment of $\Delta t = 0.005s$ are selected as the continuation of the previous work [30]. The average aerodynamic quantities are calculated in the interval of $t^* = [690 - 720]$ as well as for 20 cycles. The error is less than 0.02% for the mean values computed from the aforementioned time interval and cycles chosen. In the current study, fine mesh is also used for the highest Reynolds number and highest angle of attack investigated ($Re = 5000$ and $\alpha = 15°$). The comparative study is also conducted to investigate the accuracy and impact of turbulent models (transition k-omega SST, transition SST 4-equation) on flow characteristics at $\alpha = 6°$, $\alpha = 10°$, and $\alpha = 15°$ for $Re = 5000$. Low Reynolds correction was employed. Results are found to be trivial for laminar and the transitional turbulence models listed in Table 1 for $\alpha = 6°$.

The mean aerodynamic force coefficients values are found to be very close for lower angles of attack till $\alpha = 6°$ for different turbulence models used. However, with the increment in angle of attack ($\alpha = 15°$), the viscous laminar flow model is not able to predict the results, and at $\alpha = 10°$, SST 4-equations model has higher discrepancy than k-omega SST and laminar flow models. However, additionally, SST 4-equation model takes more computational time than k-omega SST. In the current work, k-omega SST model is used to obtain numerical results for $Re = 5000$ as compared to lower Reynolds number considered. The similar behavior of data is available for NACA0012 in the case of $Re = 4000$ at $\alpha = 10°$ [30]. The numerical results are also compared with the experimental data obtained by Sunada et al. [31] included as well in Cleaver et al. [32]. The aerodynamic forces of 15 different airfoil shapes were measured experimentally in a water tank using a load cell, including the NACA0012 airfoil at $Re = 4000$.

III. RESULTS

Two-dimensional simulations for flow over NACA0005 are performed for $\alpha = 0° - 15°$ and $Re \in [1000\text{-}5000]$. The results are obtained with $\alpha = 1°$ increment. Mean aerodynamic parameters such as lift and drag coefficient along with pressure distributions and Strouhal number are analyzed. The interaction between the angle of attack and the Reynolds number complicates the wake characteristics behind the airfoil. Several modes discovered in literature are also reported along with the discovery of new modes. The comparative values of the mean lift and drag coefficients are presented in Figure 2. The lift coefficient is found to have similar values till $\alpha = 5°$ for the Reynolds number [1000-5000] [33].

A. MEAN AERODYNAMIC PROPERTIES

$\alpha = 9°$, $\alpha = 7°$, and $\alpha = 6°$ referred as critical angles as onset of vortex shedding is noticed with increment in the angle of attack for Re = 1000, 2000, and 5000 respectively. Sharp change in C_l is observed at the critical angles of attack for $Re = 5000$ and at $Re = 2000$ for transition mode. In association with a sudden increase in the lift coefficient, drag coefficient is found to decrease for the Reynolds number 5000 as well as stall is also observed at $\alpha = 13°$. However, increment in α does not affect the C_l in case of $Re = 1000$ and the wake remains laminar in contrast to other Re values. As the angle of attack is excessive, the surface flow becomes turbulent, resulting in a sudden loss of lift, and a subsequent decrease in lift is noticed for $Re = 5000$ at $\alpha = 12°$ followed by $Re = 2000$ at $\alpha = 14°$ respectively. Similar behavior of sudden increase in lift coefficient at critical angles could be observed for $Re = 3000$ and 5000 categorized as jumps [33].

Reynolds number variations can affect the stall behavior of airfoils. At higher Reynolds numbers, thicker airfoils experience a delay in stall due to delayed separation, influencing the shedding of vortices and altering the vortex street pattern. The stall is observed by Kurtulus for NACA0012 at $Re = 1000$ at higher angles of attack [7]. Present data is found to be in good agreement with the data present in literature for $Re = 1000$ and $Re = 2000$ for lift coefficient [26], [34], [35] (Fig. 3). The correlation between Re and mean aerodynamic coefficients is shown in Fig. 4. With the increment in Re from 1000 to 5000 for lower $\alpha \leq 5°$, the coefficient of drag decreases. Similar trend is observed for the lift coefficient. Till $\alpha \leq 5°$, decline in C_l values is noticed as Reynolds number increases from 1000 to 5000. Similar trends were observed by Naeem et al. [6] and Kurtulus [30]. For $\alpha = 6°$, a transition occurred at $Re = 5000$ due to vortex shedding in wake until 9° angle of attack. Hence, at $\alpha = 9°$ higher drag coefficient results are found for $Re = 5000$ results as compared to $Re = 2000$. In comparison to both Reynolds number 2000 and 1000 cases, the mean drag coefficient is dramatically increased for $Re = 5000$ at $\alpha = 10°$.

The lower drag coefficient signifies reduced resistance, enabling smoother motion of airfoil. A slight increment in AOA and Re intensifies the flow velocity or reduces vortex separation at lower angles of attack. Wake flow is categorized into several regimes associated with the lift and drag values. Furthermore, the lift to drag coefficient is calculated to examine the effect of Reynolds number on the performance of an airfoil (Fig. 6). The lift-to-drag ratio represents the efficiency of an airfoil in generating lift relative to the drag it experiences. A high lift-to-drag coefficient denotes that the generated lift outweighs the drag experienced by the object and is desired. In aerodynamics, reduced viscosity leads to prominent vortex shedding and higher lift production. Additionally, the interplay between lift and drag becomes more pronounced. Achieving a favorable high lift-to-drag ratio is a prime objective of aerodynamics studies. In this comparative study of Reynolds number, the optimum lift to drag ratio is observed at $\alpha = 6°$ for $Re = 5000$ for the NACA0005 profile. Airfoils with higher thicknesses (NACA0006, NACA0012, and NACA0018) exhibit a modest decrease in mean lift coefficient as compared to NACA0002, for Reynolds number of 1000. For NACA0002 the highest $\frac{\bar{C}_l}{\bar{C}_d}$ value is 4.5 at $\alpha = 7°$ (Fig. 5) and for NACA0005, $\frac{\bar{C}_l}{\bar{C}_d}$ value is 3.9 at $\alpha = 7°$ (Fig. 6). As the angle of attack increases, $\frac{\bar{C}_l}{\bar{C}_d}$ decreases and the effect of airfoil thickness and Re diminishes as shown in figures 5 and 6. Both lift and drag coefficients oscillate at relatively large amplitudes at angles of attack higher than the critical angles in comparison to smaller angles of attack. In light of these phenomena, further study is needed, as the present study is limited to the results where the laminar solutions and turbulent results are very similar (Table 1). Figure 6 shows that the lift to drag ratio is highest at $\alpha = 6°$ for $Re = 2000$ and 5000 cases examined. Table 2 lists the optimum lift to drag ratio with respective angle of attack for $Re = 1000$, 2000, and 5000. Mean coefficient of pressure $\bar{C}_p = \frac{p-p_\infty}{0.5\rho U^2}$ is calculated to evaluate the adverse pressure effect of airfoil regarding Re and angles of attack (Fig. 7).

TABLE 2. Comparative results for laminar and turbulence models at $\alpha = 6°$, $\alpha = 10°$ and $\alpha = 15°$.

	$Re = 1000$	$Re = 2000$	$Re = 5000$
$\bar{C}_l/\bar{C}_d$	3.9014	5.1034	8.1641
α_{max}	7^o	6^o	6^o

It can be observed that at a fixed Reynolds number, variations in the angle of attack can influence the airflow behavior over the airfoil's surface. However, within certain limits, changes in the angle of attack primarily affect the interaction between airflow and the upper surface, altering the pressure distribution and lift generation without significantly impacting the pressure conditions on the lower surface. At low Reynolds numbers, the laminar boundary layer is more susceptible to separation, amplifying the importance of increasing angles of attack on suction pressure variation.

The laminar boundary layer is inherently more prone to separation compared to a turbulent boundary layer, exacerbating the adverse pressure gradient effects, and leading to earlier stall conditions in case of growing Reynolds number. As the angle of attack continues to rise, the separated

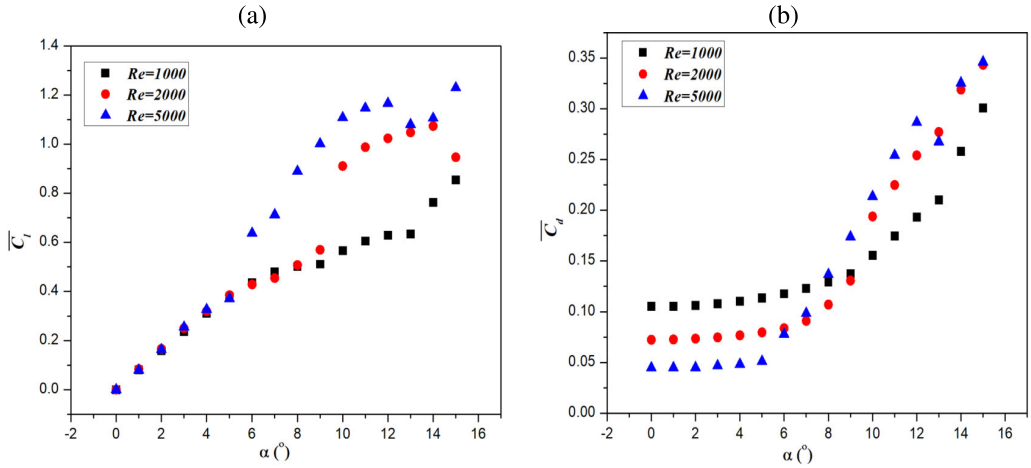

FIGURE 2. Mean values of (a) lift coefficient (C_l) and (b) drag coefficient (C_d) versus angles of attack (0° − 15°) for $Re = 1000$, 2000 and 5000.

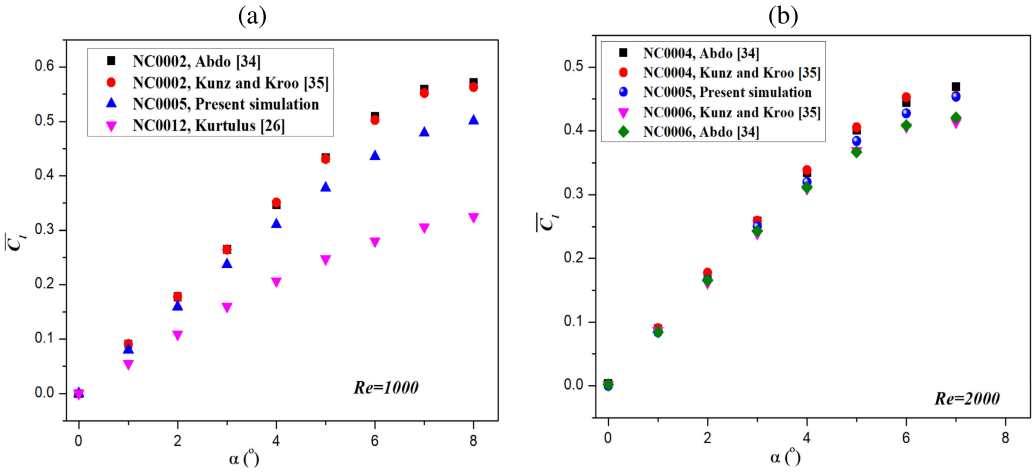

FIGURE 3. (a) Comparative values for mean lift coefficient (C_l) with literature at $Re = 1000$ and (b) comparative values for mean lift coefficient (C_l) with literature at $Re = 2000$ for angles of attack 0° − 8°.

flow region grows which intensifies the pressure difference between the upper and lower surfaces of the airfoil. This pressure differential contributes to the generation of lift but beyond a certain point, the airflow becomes fully separated causing a sudden and significant drop in lift and a sharp increase in drag—an event commonly known as aerodynamic stall. This pressure differential, attributed to the thickness airfoil contributes significantly to the coefficient of lift as compared to thin airfoils shown in figures 2 and 3. There is a higher-pressure distribution on the suction side of mode IV as can be seen in Fig. 7 for higher Reynolds numbers concerning $Re = 1000$. It represents the presence of bifurcations discussed by Rossi et al. [22].

By increasing Re and the angle of attack, the airflow encounters adverse pressure gradients, particularly on the upper surface of the airfoil. This adverse pressure gradient causes changes in the airflow pattern, leading to boundary layer separation and a subsequent decrease in suction pressure on the upper surface. Additionally, increased angles of attack still induce adverse pressure gradients that can cause premature flow separation on the upper surface (Fig. 13). As a result, the suction pressure decreases on the upper surface as the angle of attack continues to rise. Conversely, the suction pressure on the lower surface, initially higher due to its curvature, might also experience changes as the angle of attack increases for $Re = 5000$ (Fig. 7c).

As a result of the vortex shedding phenomenon, peaks are observed in the frequency spectra for the lift force. As the angle of attack increases for $Re \in$[1000-5000], the amplitude of the oscillation for the aerodynamic coefficients increases rapidly. In Fig. 8, dominant and subharmonic frequencies are determined for various angles of attack by applying the Fast Fourier transform (FFT) at the instantaneous lift coefficient. Additionally, the critical angle where oscillations of the aerodynamic force coefficients start and vortex shedding occur along with the dominant frequencies derived from amplitude spectrum of C_l are listed in Table 3. As Reynolds increases from 1000 to 5000, the critical angle is found to decrease from 9° to 6°. However, the frequency of oscillations increases from 1.42Hz to 7.72Hz.

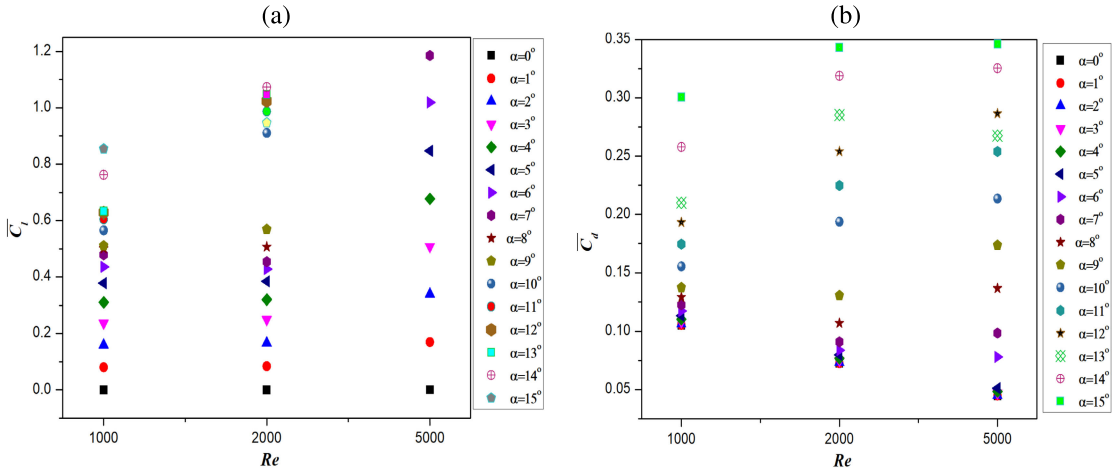

FIGURE 4. Mean values of (a) lift coefficient (C_l) and (b) drag coefficient (C_d) versus $Re = 1000$, 2000 and 5000 for increasing angles of attack.

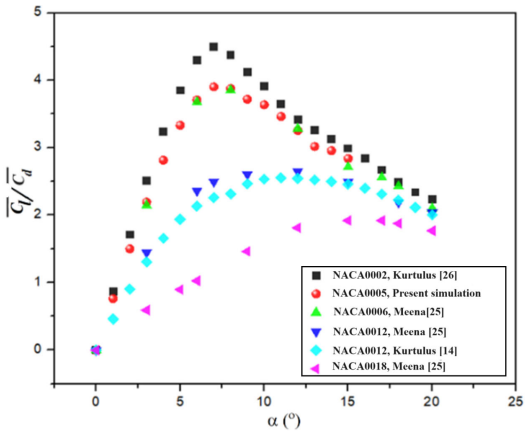

FIGURE 5. Comparative mean values of lift coefficient to drag coefficient ratio for different 4-digit symmetric airfoils at $Re = 1000$ versus angles of attack.

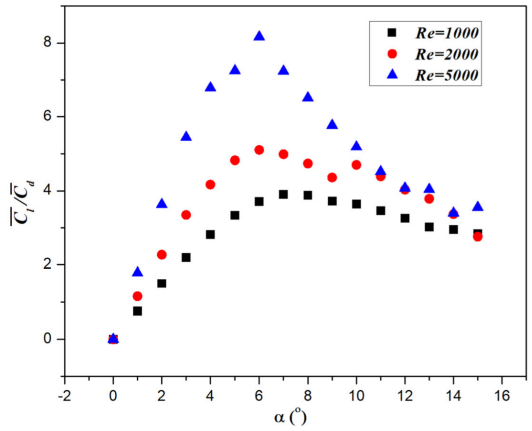

FIGURE 6. Mean values of lift coefficient to drag coefficient ratio values for NACA0005 with increasing angles of attack and Reynolds numbers.

TABLE 3. Critical angles of attack and dominant frequencies for different reynolds numbers.

	$Re = 1000$	$Re = 2000$	$Re = 5000$
critical angle of attack	9^o	7^o	6^o
Dominant Frequency (Hz)	1.42	4.59	7.72

Table 4 presents the critical angles for various 4-digit NACA profiles with varying Reynolds numbers. For regular pattern of vortex shedding at lower angles of attack and Reynolds number. The Strouhal number $St = \frac{fc}{U}$ decreases with the increase in angle of attack for a fixed Reynolds number. It is noted that lower angles of attack tend to delay flow separation, resulting in a longer and more continuous shedding of vortices. This increased shedding frequency affects the Strouhal number by elevating the oscillation frequency component. The shedding frequency f_1 denotes the primary shedding frequency (single peak) for dominant vortices. Based on f_1, transition process of boundary layer, several small-scale vortices appear upstream of separation. The subharmonics were also well visible in terms of higher frequency components as $2f_1$, $3f_1$,..., with lower intensities in the spectrum. Critical angle in aerodynamics is determined based on onset of vortex shedding. Due to the growth of laminar separation bubble, disturbance in wake is noticed for angles of attacks below critical angles. Over critical angles of attack where oscillations occur, both the lift and drag coefficient amplitudes tend to grow with growing Reynolds number. There is a strong correlation between α, Re, and vortex shedding (Durante et al. [20], Rossi et al. [22], Kunz and Kroo [35], Kurtulus [36]).

At lower α, the airflow over the airfoils is relatively undisturbed, and the lift generated is usually efficient. However, with increasing angle of attack, the airflow separates from the foil surface, creating low pressure regions on the upper surface and high pressure regions on the lower surface. Angles of attacks 7°, 9°, 10°, 13°, and 15° are selected to analyze the instantaneous and mean, non-dimensional vorticity contours, instantaneous and mean streamlines figures (11-15), and C_l coefficients (Fig. 16). Separation bubbles occur when

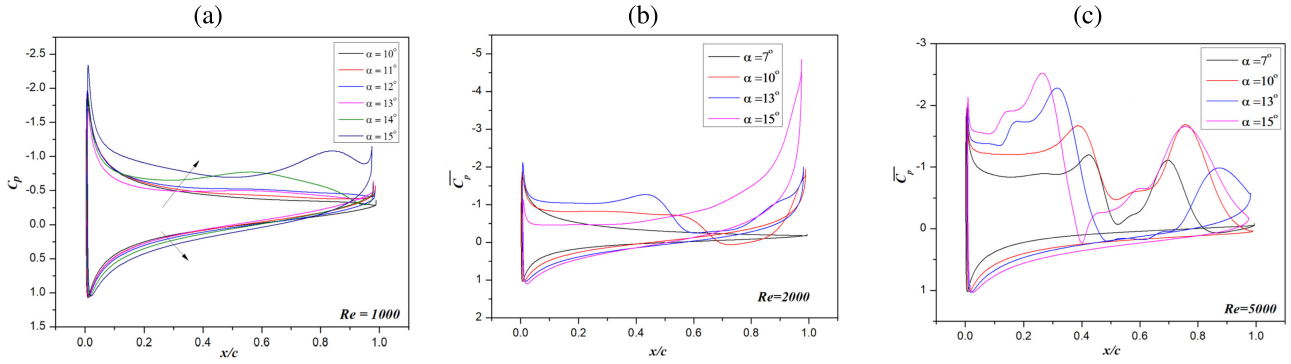

FIGURE 7. Mean C_p curves for the various angles of attack for (a) $Re = 1000$, (b) $Re = 2000$, and (c) $Re = 5000$.

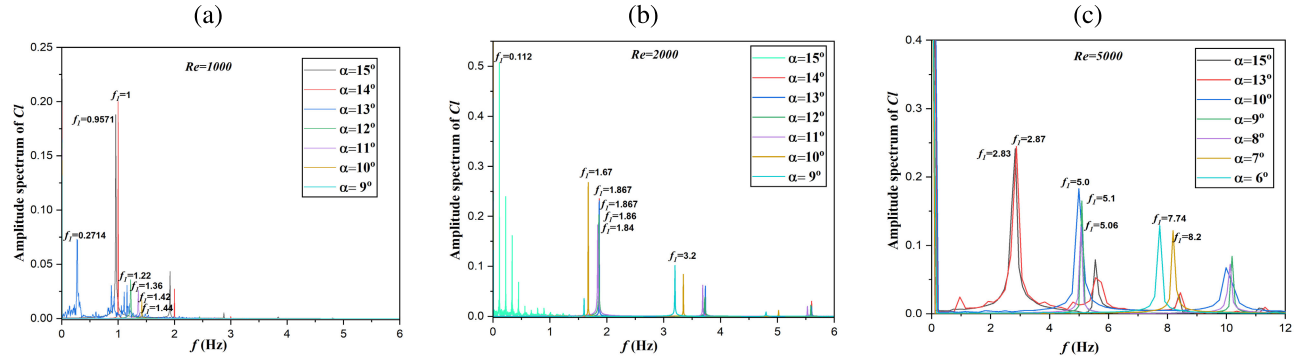

FIGURE 8. Amplitude spectrum analysis for the various angles of attack for (a) $Re = 1000$, (b) $Re = 2000$, and (c) $Re = 5000$.

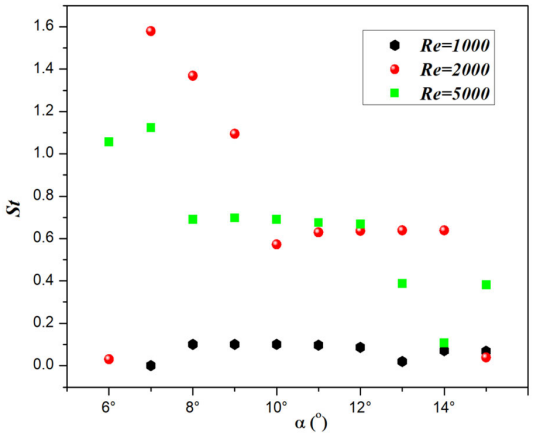

FIGURE 9. Strouhal number versus various angles of attack for (a) $Re = 1000$, (b) $Re = 2000$, and (c) $Re = 5000$.

the boundary layer flows over an airfoil separates from the surface, creating a region of reversed flow before reattaching downstream. Flow separation begins when the boundary layer separation and formation of separation bubble, altering the pressure distribution and causing the flow to separate.

IV. FLOW FIELDS AROUND NACA0005

A. CONTINUOUS VORTEX SHEDDING MODE (MODE I)

For lower angles of attack, there is a smaller pressure difference between the upper and lower surfaces of the airfoil (Fig. 7). This relatively symmetrical pressure distribution contributes to the favorable lift-to-drag ratio seen in this regime (figures 5 and 6). Compared to other unsteady vortex modes, the airfoil experiences the least amount of drag in this flow regime. At the smaller angles of attack, the boundary layer (a thin layer of air adjacent to the surface of airfoil) remains relatively attached, reducing separation and turbulence (figures 10 and 11). This attachment aids in maintaining a more streamlined airflow and minimizing drag

TABLE 4. Critical angles of attack for 4-Digit symmetric airfoils versus Reynolds number.

Airfoil	Reynolds number	Critical angle
NACA0002, Kurtulus [7]	1000	$8^o \leq \alpha \leq 9^o$
NACA0002, Kunz [35]	2000	$\alpha \geq 5.5^o$
NACA0002, Kunz [35]	6000	$\alpha \geq 4^o$
NACA0002, Kunz [35]	2000	$8^o \alpha \geq 7^o$
NACA0005, Current study	1000	$\alpha \approx 7^o$
NACA0005, Current study	2000	$\alpha \approx 9^o$
NACA0005, Current study	5000	$\alpha \approx 7^o$
NACA0006, Meena [25]	1000	$8^o \leq \alpha \leq 9^o$
NACA0006, Kunz [35]	2000	$\alpha \geq 7.5^o$
NACA0008, Pranesh [37]	1000	$\alpha = 6^o$
NACA0010, Rossi [22]	1000	$\alpha = 10^o$
NACA0010, Rossi [22]	250	$\alpha = 30^o$
NACA0012, Kurtulus [7] Kouser et al. [15]	1000	$\alpha = 8^o$, $8^o \leq \alpha \leq 9^o$
NACA0012, Kurtulus [30]	2000	$5^o \leq \alpha \leq 6^o$
NACA0012, Kurtulus [30]	4000	$3^o \leq \alpha \leq 4^o$
NACA0015, Menon [38]	500	$\alpha = 12.5^o$
NACA0015, Menon [38]	2000	$\alpha = 5^o$
NACA0018, Meena [25]	1000	$\alpha = 6^o$

generally provides better lift-to-drag ratios. In this study, for $\alpha = 0°$, the flow is attached and steady in case of $Re = 1000$. While no disturbance occurred the surrounding flow and remains practically steady laminar flow. Furthermore, in the case of steady state, at the lower angles of attack, the airflow over the airfoil tends to remain attached except generation of a small trailing edge bubble which develops and grows in length as angle of attack increases. The coefficient of drag behaves differently at lower angles of attack. C_d tends to be relatively low due to the relatively undisturbed airflow and the reduced formation of drag-inducing phenomena like separation and turbulence.

The laminar flow and the attachment of the boundary layer contribute to this lower C_d value. However, for Reynolds numbers 2000, and 5000 the wake flow appears to be locally stable up to $\alpha = 6°$, and $\alpha = 5°$ respectively (figures 10 (a) and (b)). This state is termed as Mode I or S [39]. When steady flow transitions to oscillatory flow, it experiences a supercritical Hopf bifurcation [33]. As a result, wake instability starts at $\alpha = 7°$ for $Re = 2000$, and $\alpha = 6°$ for $Re = 5000$ instead of $\alpha = 9°$. Until reaching the critical angles of attack, the flow behaves similar to $Re = 1000$. With increasing AOA, wake instability tends to develop closer to the trailing edge of the airfoil, and at $\alpha = 5°$, it occurs in its immediate vicinity. No reattachment on the upper surface can be observed. The shedding phenomenon is observed at $\alpha = 6°$ and $\alpha = 7°$ for $Re = 5000$ and 2000 respectively (figures 10 and 11). At first, with the increment in angle of attack, the separation bubble increases. Counter-rotating vortices grow and become more visible. A periodic wake with one dominant wavelength (frequency) appears downstream of the airfoil on slight increment in α, known as Von-Karman vortex street (alternating pattern of swirling vortices trailing behind the airfoil).

B. ALTERNATING VORTEX SHEDDING MODE (MODE II)

At the same angle of attack but for different Reynolds numbers, the thickness effect on these modes can be observed clearly. For higher thickness airfoil, these modes are observed for higher angles of attack [14], [15], [22], [25]. Figure 11 represents the instantaneous, mean non-dimensional vorticity contours for $\alpha = 7°$. Decreasing Reynolds number enhances the effects of increased boundary layer thickness, and increasing angle of attack accelerates trailing edge separation from higher to lower Re [34].

At a low Reynolds number of 1000, the wake is steady laminar as compared to the higher Re. The growth of separation bubbles is influenced by α as well as Reynolds number. Growth of the separation bubble is observed with a lower magnitude near the trailing edge of the airfoil as a result wake remains attached. This phenomenon is also observed by Kurtulus [36], and Kouser et al. [15] for NACA0012. According to the mean streamlines, the mean separation point moves toward the leading edge as angle of incidence increases, and the separation bubble covers half of the upper surface of airfoil. Airfoils are subject to this phase based on the unperturbed flow field over the surface. Alternatively, when the velocity gradients become larger, the two vorticity sheets interact, forming an ordered vortex street. These vortices have varying sizes and strengths, and they persist downstream, creating a distinctive pattern resembling a series of interconnected rings or loops, and swirling eddies. This ordered vortex shedding is at $\alpha = 9°$, $\alpha = 7°$, and $\alpha = 6°$ for $Re = 1000$, 2000, and 5000 respectively (figures 10,11, and 12). This is called phase 2S (William and Roshko [39]) or named Mode II (Kurtulus [26]).

An increase in C_l value is observed with the onset of unsteadiness (Fig. 2). Increasing mean C_l with Reynolds number is caused by the formation and shedding of a leading-edge vortex [38]. At this stage, the fluid tends to exhibit less resistance to deformation and flow, resulting in thinner boundary layers around the object. Thinner boundary layers lead to the shedding of vortices that are smaller in size and closer together in the wake. For the $\alpha = 7°$, the difference in mean and instantaneous wake is also observed. The wake is more stable and developed at this stage. However, for Reynolds number 5000, reattachment in the middle of chord length can be noticed as compared to the lower Re considered. Two clockwise bubbles grow on suction side of airfoil with different magnitudes. Hence the two wakes are observed behind the trailing edge with noticeable differences. A larger spatial separation is observed between two vortex pairs in the 2S mode than Mode I. Similar to $\alpha = 7°$ for $Re = 2000$, Von-Karman vortex street is observed at $\alpha = 9°$ for $Re = 1000$. Instantaneous streamlines show the growth of separation bubble and shedding of clockwise and counterclockwise vortices downstream whereas mean streamlines depict the growth of separation bubble and separation of layer towards the leading edge.

C. MODE III

At $\alpha = 10°$, during the regime shift, the contour lines of vorticity are elevated above the center of the wake, which exhibits the decline of lift experienced by the airfoil at $Re = 2000$ and 5000. In comparison to the Mode II regime, the height of the wake increases considerably. Shear layer is swallowed up and a diapole is detached in the upward direction of wake (Fig. 11(c)). It is also termed as rightward vortex shedding mode observed by Gupta et al. [33] at $Re = 5000$ for $\alpha = 8°$. Figures 12(c) and 13(c) represent the mode III (category iii) with higher intensities and wake becomes more thicker as compared to the lower angles of attack. These chaotic alternating vortices reported by Gupta at $\alpha = 15°$ for $Re = 5000$. However, in case of NACA0005, these modes are observed at $\alpha = 9°$ and $\alpha = 10°$. As the airfoil goes through Mode III, there is a dominant single wavelength with concentrated vortices. This phenomenon is explained well by Rossi et al. [22].

The airfoil experiences a greater drag force as a result. Mode III was closely investigated by Kurtulus [26] by careful evaluation of time histories of the lift and drag coefficients, Poincaré maps, and the instantaneous vorticity contours.

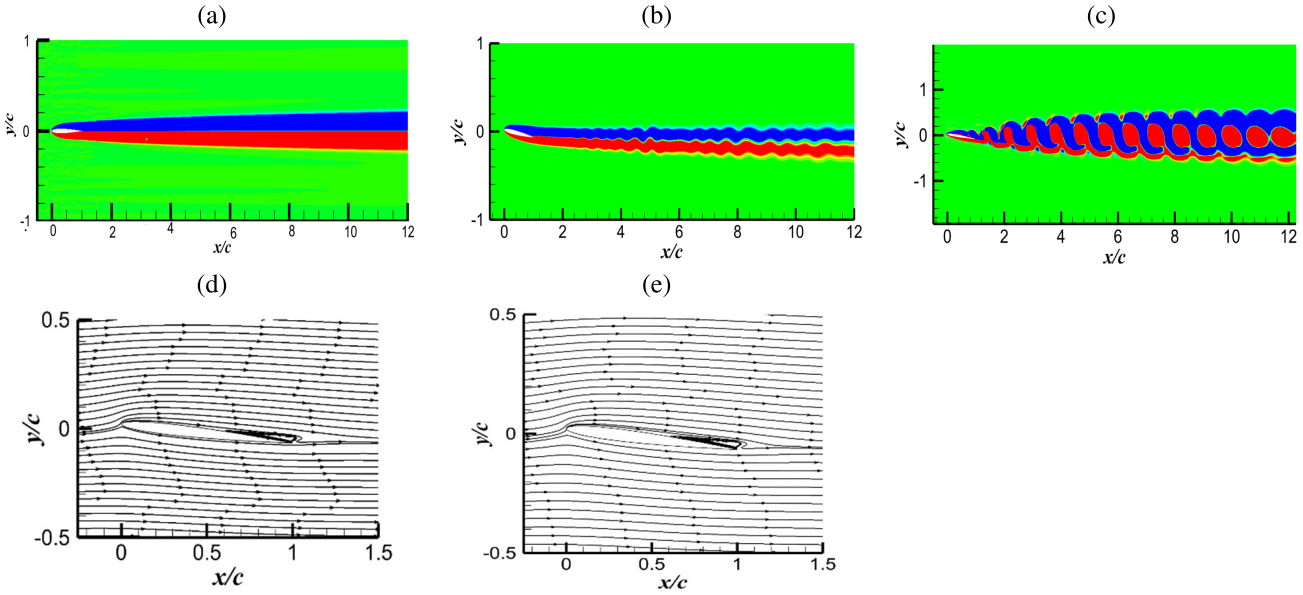

FIGURE 10. Transition from Mode I to Mode II at $Re = 5000$. Red and blue color show the counterclockwise and clockwise vortices for $\omega c/U = -1$ to 1 respectively. Figure represents (a,b) Mode I, (c) Mode II, and (d) and (e) instantaneous and mean streamlines at $\alpha = 5°$.

During the alternating vortex pairs shedding mode (Mode III), pairs of counter-rotating vortices alternate between an upper and lower branch. The wake thickness increases as the angle of attack further deviates from the ideal angle for attached flow, causing greater separation and a larger wake region. A larger wake height reflects increased drag experienced by the airfoil compared to the steady regime observable from the averaged vorticity fields.

D. MODE IIIA/C

Mode IIIa/c is first reported by Durante et al. [20]. This new mode is a switching state of Mode III observed as a completely chaotic wake behind the trailing edge. This mode III(a/c) is also captured in NACA0005 at the lower angle of attack 13° than 25° reported in Naeem et al. [6] work. The Poincaré map and amplitude spectrum of the lift coefficient capture the chaotic nature of this time bifurcation phenomena. Due to the interactions between the vortex couples, flow behavior repeatedly changes between two categories, resulting in an unorganized wake. If the analysis domain were longer, then this chaotic behavior would be captured more clearly in the wake patterns. The flow behavior can be seen repeatedly change between two categories resulting in an unorganized wake due to the interactions between the vortex couples.

Vortex shedding at varying angles of attack with different airfoil thicknesses exhibits diverse characteristics. Thicker airfoils might experience changes in the shedding frequency or the symmetry of the vortex street pattern at higher angles of attack. The vortices may become more pronounced or irregular, impacting the aerodynamic performance of the airfoil.

E. MODE 4I

A new state of alternating single vortex with vortex pair shedding mode discovered by Naeem et al. [6] is also observed in the current study for the $Re = 2000$ at angle of attack 10°, 13° and 15°. These modes were observed at angle of attack 10° during the investigation of NACA0002 for the Re ranging from 100-3000. Unlikely mode III (similar to P), figures (13(b), 14(b), and 15(b)) show that mode 4i has two branches of vortices. However, the dipole shed in upper branch of wake has low movement in the upward direction and after a distance, it becomes weak as compared to mode III. The lower branch does not have clockwise vortices. mode 4i is more likely to mode IV but with different vortex spin direction having narrow wake thickness. The mean vorticity contours represent the inverted clockwise and counterclockwise vortices present in the wake. Furthermore, mode 4i has higher dominant frequency of 0.6 U/c as compared to mode IV with 0.4 U/c frequency [6]. In our investigation, the dominant shedding frequency is 0.58 U/c and 0.63 U/c for 10° and 13° (figures 8 and 9). However, the frequency is sharply dropped indicating a bifurcation. Instantaneous vorticity contours as well as streamlines show the formation of vortex. The instantaneous formation of the vortex formation is given in detail by Naeem et al. [6]. On the suction side of the airfoil, there is one large clockwise (CW) vortex attached to the leading edge and one counterclockwise (CCW) vortex attached to the trailing edge. The CW vortex is driven toward the trailing edge of the airfoil by the CCW vortex that is formed near the leading edge on the suction side. The vortex is pushed more toward the rear of the airfoil. As the CCW vortex pushes upward, it divides the large CW vortex into two smaller ones.

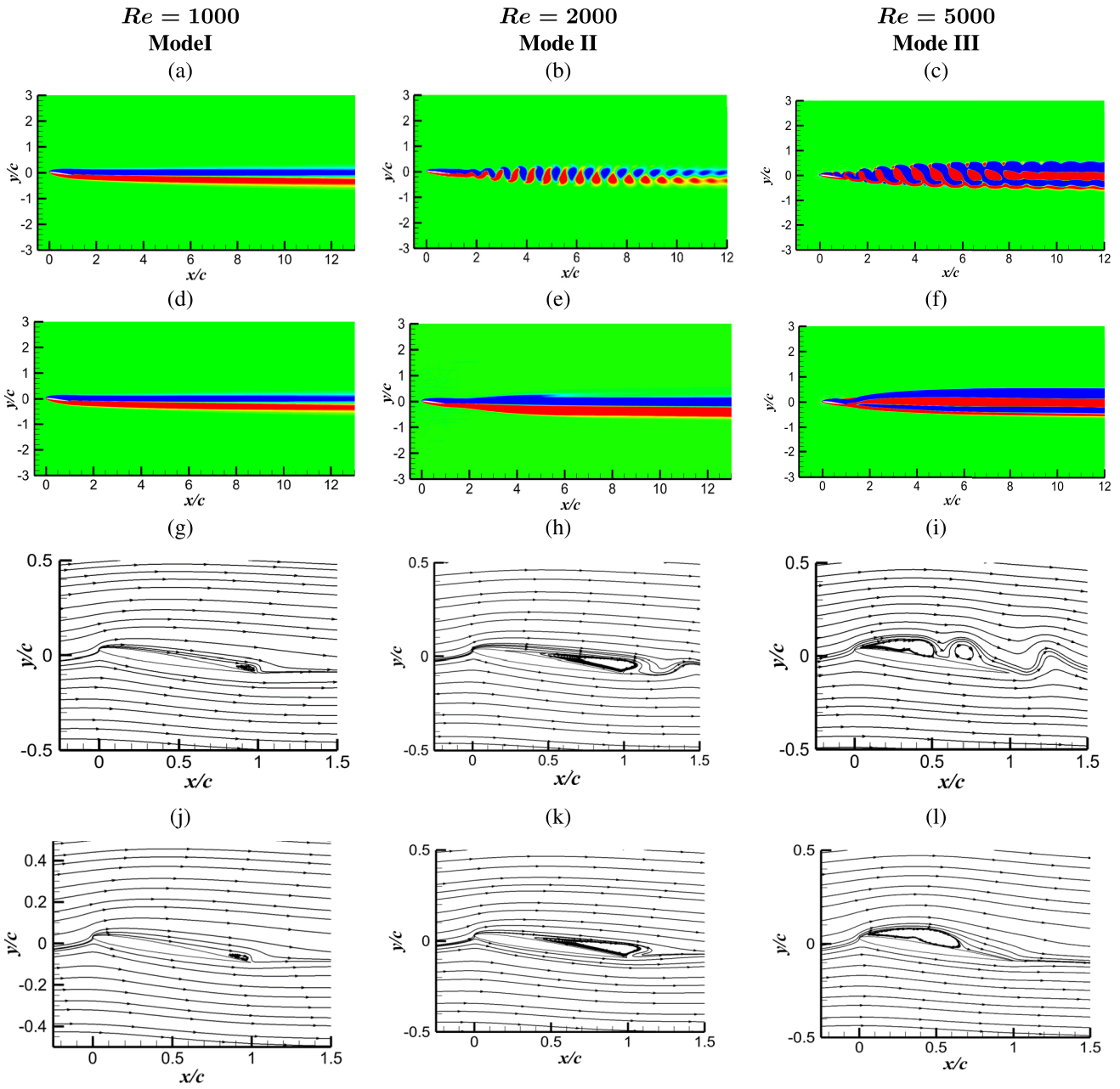

FIGURE 11. Wake shed by NACA0005 at $\alpha = 7°$. (a,b,c) Instantaneous vorticity countors, (d,e,f) mean vorticity countors, (g,h,i) intantaneous streamlines, and (j,k,l) mean streamlines at $\alpha = 7°$ with respect to $Re = 1000$, 2000 and 5000 respectively. Non-dimensional vorticity contours $\omega c/U$ are plotted for -1 to 1. Red and blue colors show the counterclockwise and clockwise vortices.

A small CW vortex remains attached to the airfoil while the other moves upward and rearward. A CW vortex attached to the suction surface near the trailing edge merges with two smaller unequal CW vortices. Meanwhile, the CCW vortex positioned at the trailing edge at an instant is divided by merged CW vortex at instant. A pair of CCW vortices on the upper branch of the wake, with one attached to the trailing edge and the other pushed upward and rearward. In the upper branch of the wake, the largest of the two unequal CW vortices moves upward and rearward. During the split in CCW vortices, one remains attached to the trailing edge and the other is pushed upward and rearward, resulting in the pair of vortices on the upper branch of the wake. A more detailed analysis of CCW can be found in [40] and [41].

F. K-MODE

For angle of attack 15° (Fig. 14 (b)), the mode becomes more developed, and it may be a transition stage to another mode. However, due to the domain size, it is not possible to visualize here, and the study would be the next goal of our research.

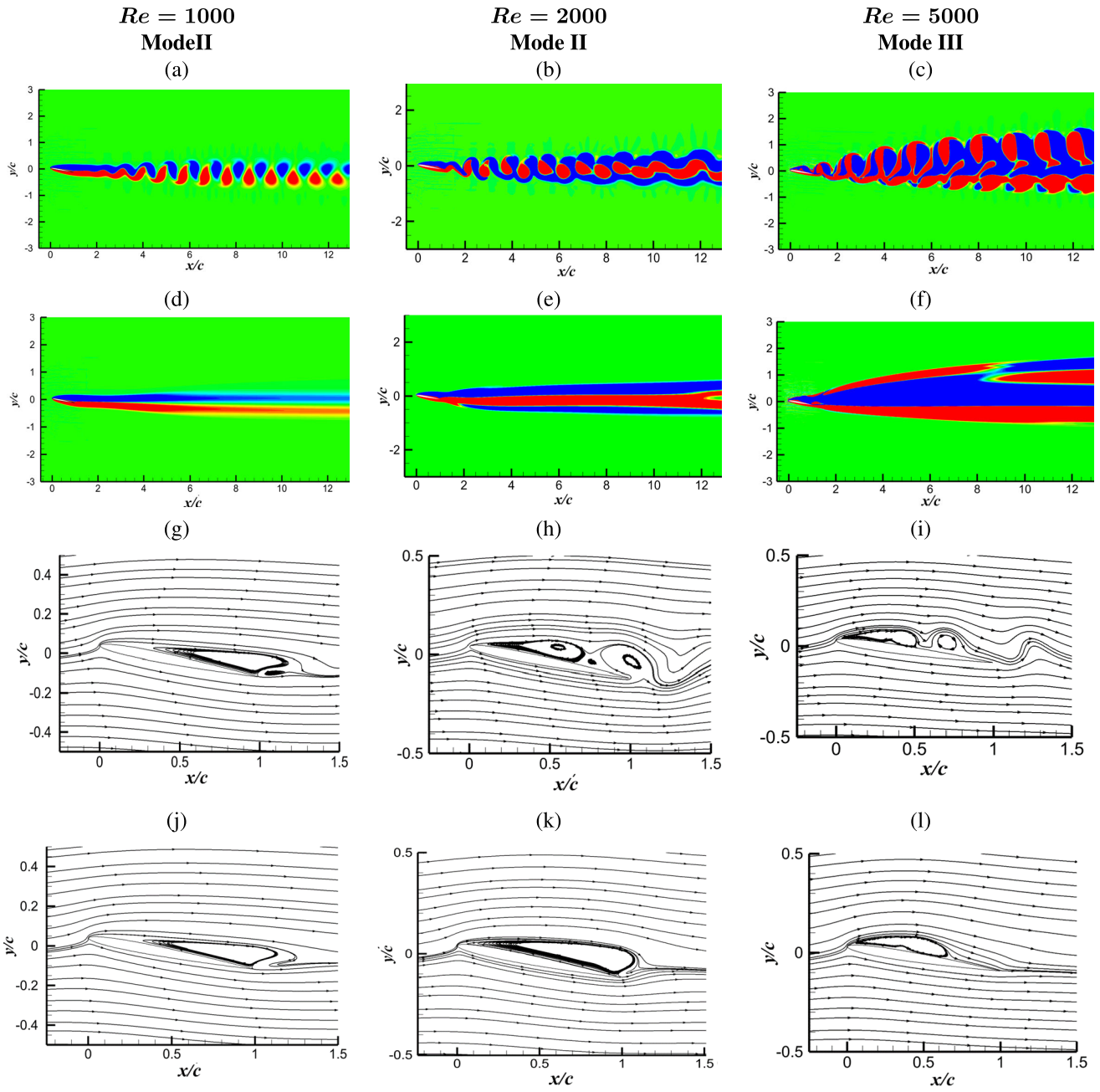

FIGURE 12. Wake shed by NACA0005 at $\alpha = 9°$. (a,b,c) Instantaneous vorticity countors, (d,e,f) mean vorticity countors, (g,h,i) instantaneous streamlines, and (j,k,l) mean streamlines at $\alpha = 9°$ with respect to $Re = 1000$, 2000 and 5000 respectively. Non-dimensional vorticity contours $\omega c/U$ are plotted for -1 to 1. Red and blue colors show the counter-clockwise and clockwise vortices.

In this study, a new mode named k-mode is found at $Re = 5000$ for NACA0005 as the angle of attack is increased from 10°. This mode is most similar to the periodic doubling but a packed 2P mode. 2P mode is reported by [8], [25], and [36] at higher angles of attack in case of thicker airfoils. Few studies are available in literature for NACA0012 under Reynolds number ranging 5000-5500 [33], [42], [43], [44]. Lift force for Reynolds number 5300 was measured by a load cell technique to analyze the near wake characteristics [45]. With an increment in the Reynolds number, boundary layer separation advances towards the leading-edge figures (13,14, and 15) (c)).

Mean stream vorticity shows that the separation bubble grows in size and strength due to the infusing mass into the leading-edge vortex (LEV). Instantaneous vorticity contour shows a distinct reversed vortex structure begins to appear under the LEV as it grows at the leading edge which, earlier, was engulfed by the LEV. This vortex structure in the figure is known as a secondary counter-rotating vortex (SCV). At the leading edge, another vorticity is rolled up by the feeding

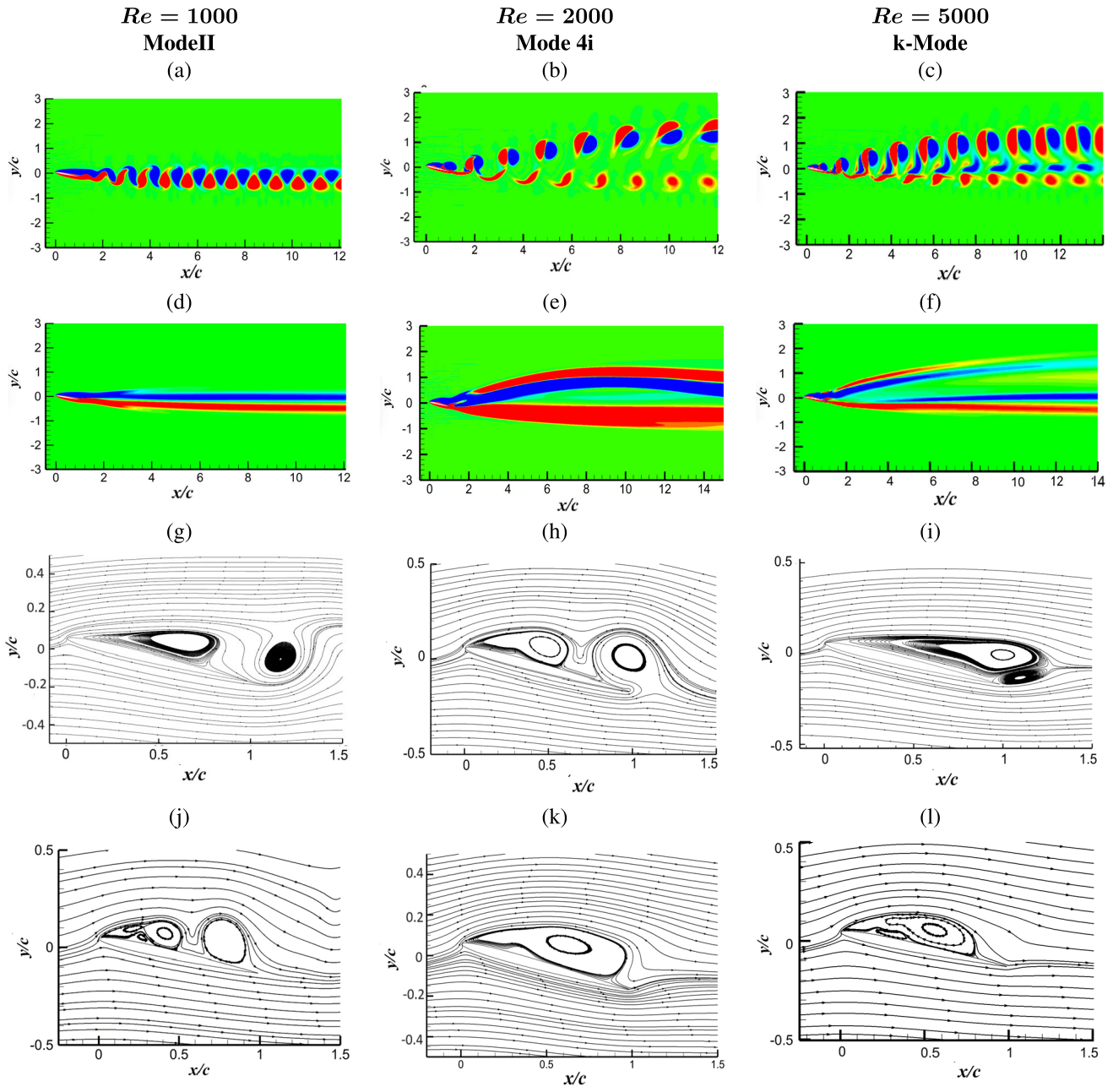

FIGURE 13. Wake shed by NACA0005 at $\alpha = 10°$. (a,b,c) Instantaneous vorticity countors, (d,e,f) mean vorticity countors, (g,h,i) intantaneous streamlines, and (j,k,l) mean streamlines at $\alpha = 10°$ with respect to $Re = 1000$, 2000 and 5000 respectively. Non-dimensional vorticity contours $\omega c/U$ are plotted for -1 to 1. Red and blue colors show the counter-clockwise and clockwise vortices.

shear layer. The growing secondary counter-rotating vortex cuts off the connection between LEV and feeding shear layer as the motion continues. This new vortex advects away along with the LEV in the wake leaving a portion behind to roll down along the top surface of the airfoil to reach the trailing edge. Two pairs are shed in the wake similar to the 2P mode. The leading edge vortex dynamics at $Re = 3000$ for NACA0012, and NACA0015 are found to be highly non-linear, noncyclical [46], [47].

As the separation type observed at the suction side of the airfoil varies, the aerodynamic forces are highly unsteady. The interaction between the shed vortices and the boundary layer of the surface of object plays a critical role in reforming the C_l and C_d patterns. By impinging on the boundary layer, vortices shedded alter the flow characteristics and subsequently affect the aerodynamic coefficients. As a result, C_d and C_l deviate from its regular periodic pattern for $Re = 5000$. Figure 7 shows that higher Re and α resulting

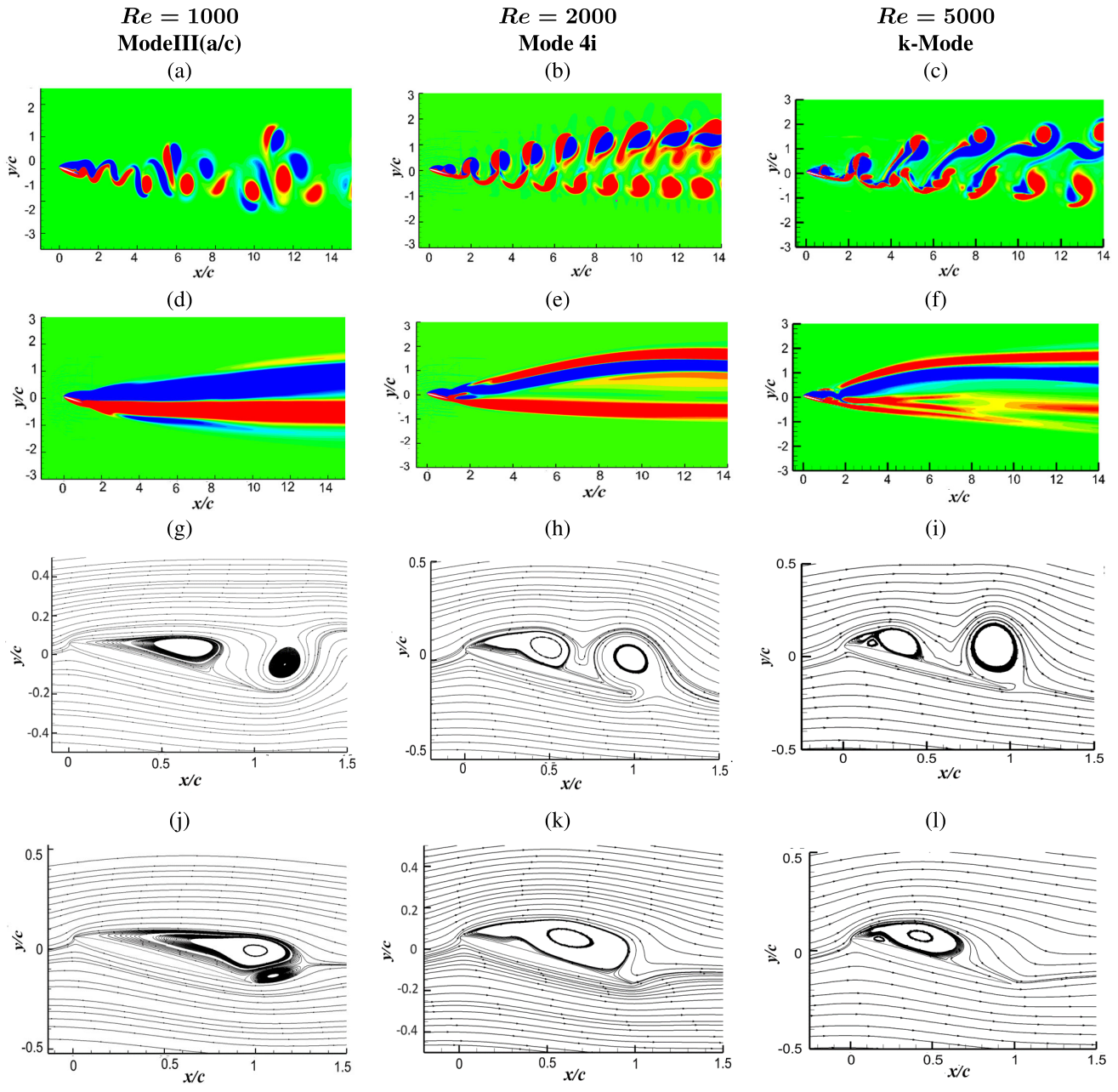

FIGURE 14. Wake shed by NACA0005 at $\alpha = 13°$. (a,b,c) Instantaneous vorticity countors, (d,e,f) mean vorticity countors, (g,h,i) intantaneous streamlines, and (j,k,l) mean streamlines at $\alpha = 13°$ with respect to $Re = 1000$,2000 and 5000 respectively. Non-dimensional vorticity contours $\omega c/U$ are plotted for -1 to 1. Red and blue colors show the counter-clockwise and clockwise vortices.

in a strong negative pressure at the suction side, both elements contribute to the formation of the vortex pair closer to the surface. ingle SCV is triggered on the upper part of surface of airfoil due to adverse pressure gradient to suppress the separation. Secondary vortex formation often occurs due to the three-dimensional nature of flow around airfoils or the presence of local flow disturbances. These secondary vortices develop as a consequence of the primary vortices interacting with these geometric irregularities or flow disruptions, leading to additional swirling motions along the airfoil surface. This leads to a change of triggered topology. The negative pressure causes the counterclockwise tip vortex to roll up and form a pair with the oncoming clockwise leading-edge vortex. There is also strong suction pressure at the trailing edge causing to break the clockwise vortices into more than two before it sheds. As a result of the strong suction pressure behind the airfoil, clockwise leading-edge vortices and distributed in the wake. This results in the randomly arranged paired and unpaired vortices as a result of all vortices being unable to form pairs. This is also identified

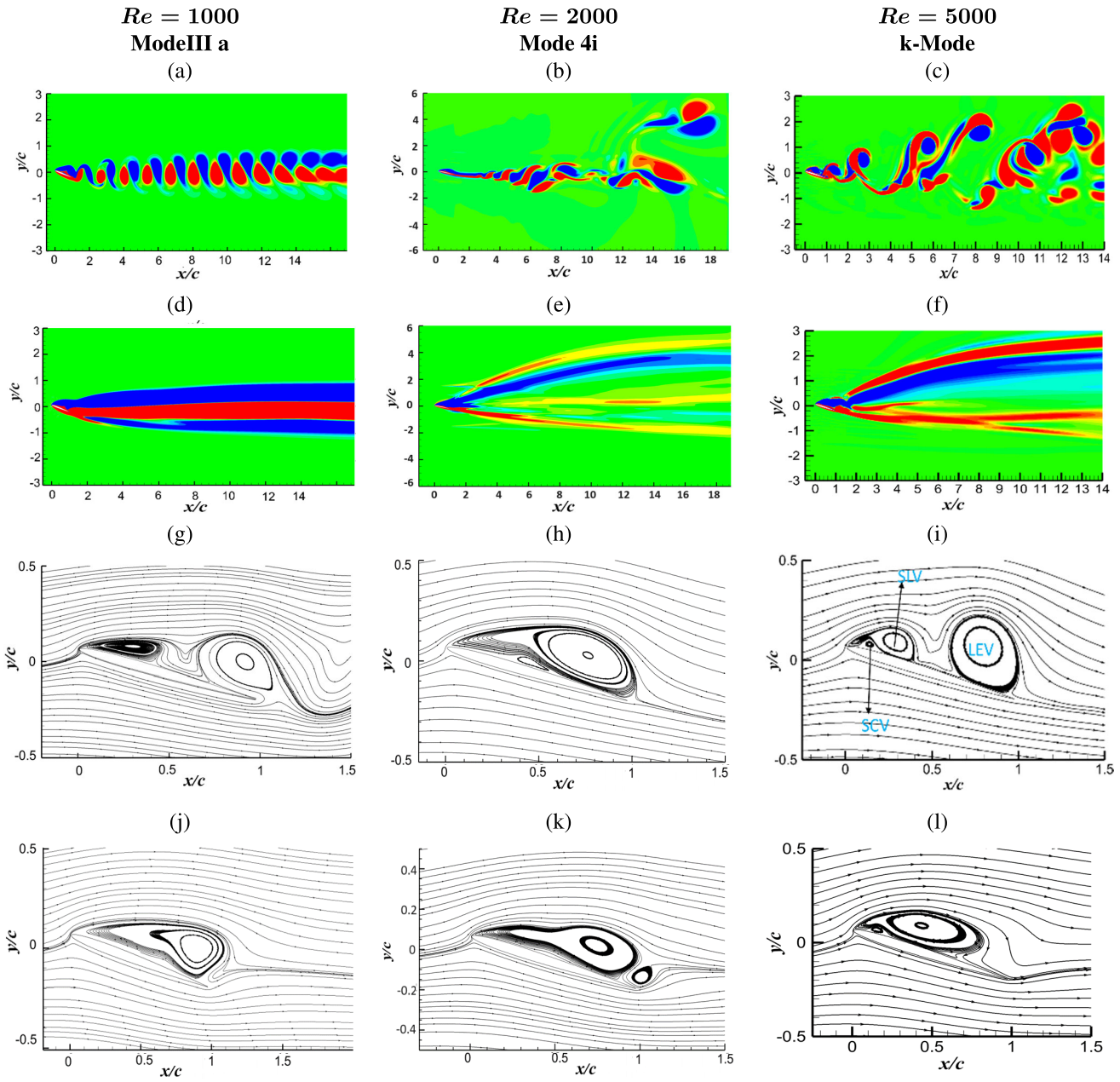

FIGURE 15. Wake shed by NACA0005 at $\alpha = 15°$. (a,b,c) Instantaneous vorticity countors, (d,e,f) mean vorticity countors, (g,h,i) intantaneous streamlines, and (j,k,l) mean streamlines at $\alpha = 15°$ with respect to $Re = 1000$, 2000 and 5000 respectively. Non-dimensional vorticity contours $\omega c/U$ are plotted for -1 to 1. Red and blue colors show the counter-clockwise and clockwise vortices.

as a chaotic form of Mode III with a strong effect of clockwise vortices figures (14(c) and 15(c)).

The noticeable difference in the wake thickness is obvious. As separation occurs, the wake thickness behind the airfoil expands. Similar vortex phenomenon is observed by using resolved analysis (Marquet et al. [44]) for angles of attack changes from $\alpha = 7° - 8°$. The wake is most prominent for the new modes reported as compared to all other regimes. Consequently, airfoils operating in this regime are therefore subject to the highest drag force of all modes. Additionally, airfoils are also subject to downward forces due to upward displacements of mean flow, which reduce lift growth. Figure 16 represents the unsteady behavior of C_l pattern and corresponding FFT analysis for the modes present at various angles of attack at $Re = 5000$. With the increment in angle of attack the main vortex shed with higher intensity. At $\alpha = 13°$, the presence of other vortex with lower magnitude could be observed and turbulence in FFT is obvious which shows the transition of mode IV to a new mode in the wake.

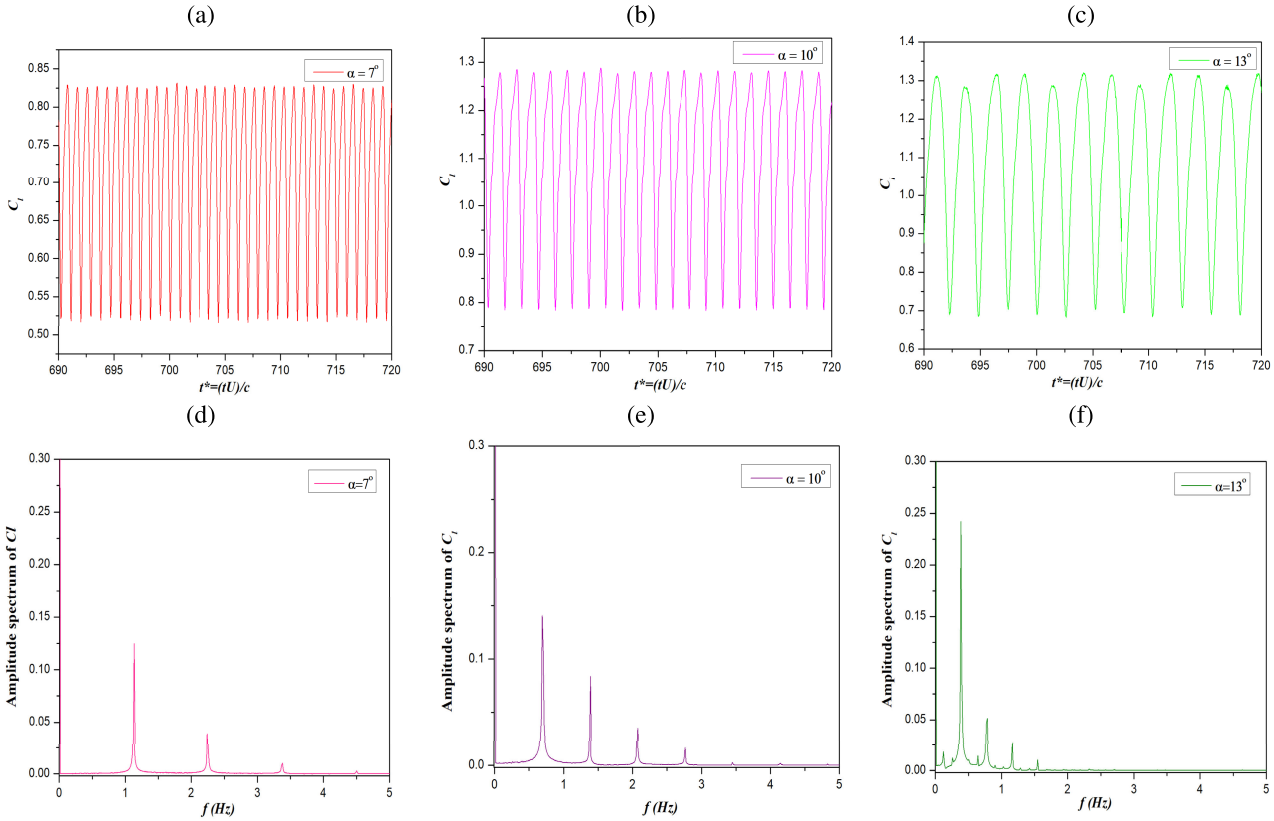

FIGURE 16. (a,b,c) intanstaneous coefficient lift behavior versus (d,e,f) frequency analysis at $Re = 5000$ for (a,d) $\alpha = 7°$, (b,e) $\alpha = 10°$, and (c,f) $\alpha = 13°$.

V. CONCLUSION

In this study, unsteady flow fields are investigated around the NACA0005 airfoil for 0° to 15° angles of attack and Reynolds number ranging [1000-5000]. Literature results are compared well with those obtained here. This paper discusses the angle of attack and Reynolds number effect on wake pattern, instantaneous, and mean aerodynamic coefficients. Furthermore, it is interesting to show how the variation in Reynolds number highly affects the vortex patterns while angles of attack remain fixed. Several modes are observed for different angles of attack and Reynolds number. Spectrum analysis is also conducted for different angles of attack.

- For $Re = 1000$, the amplitude spectrum of C_l coefficient begins to peak at 9°, and the aerodynamic forces show oscillatory behavior thereafter. The flow depicts Mode II at this stage. On further increment in the angle of attack, the flow is perturbed, and mode IIIa/c is upturned. At 15°, mode III (caterogry 1) or mode P with one pair of vortices in the upper part of wake is observed.
- For $Re = 1000$, the amplitude spectrum of C_l coefficient begins to peak at 9°, and the aerodynamic forces show oscillatory behavior thereafter. The flow depicts Mode II at this stage. On further increment in the angle of attack, the flow is perturbed, and mode IIIa/c is upturned. At 15°, mode III caterogry1or mode P with one pair of vortices in the upper part of wake is observed.
- For $Re = 2000$, the flow remains steady laminar until $\alpha = 6°$. Later on, on increasing angle of attack, it turns to mode II and eventually reaches to the recently discovered mode 4i by Naeem et al. [6] at angle of attack $\alpha = 10°$. With further increment in α, the mode 4i becomes more developed. The spectral analysis also shows the Strouhal number ranges from 0.57-0.63 for this mode.
- In case of $Re = 5000$, unsteady vortex shedding is observed at $\alpha = 6°$, the lowest angles of attack as compared to other Reynolds numbers examined for NACA0005. At $\alpha = 10°$, flow is transitioned to a new mode named as k-mode (modified 2P) mode. The dipole shed in the upper wake has the higher magnitude and same spin direction as reported before by Kouser et al. [15]. However, the vortex pair in the lower part of the wake is weak in magnitude and the spin direction is similar to the vortex pair in the upper part of wake of mode 4i. Additionally, the wake is narrow in contrast to the 2P mode. Secondary vortex generation is observed on the upper surface of the airfoil. As the angle of attack is increased from $\alpha = 10°$ to $\alpha = 13°$, the disturbance could be seen in the lift and respective frequency spectra show the transition to the state. As a result, the mode is perturbed and becomes chaotic. However, more investigation is required to fully categorize this mode.

Spectral analysis shows the subharmonic frequency peaks for higher angles of attack for every Reynolds number considered. Each fixed $\alpha \geq 10°$, shows the presence of different modes with variation Reynolds number. Thus clearly presents the effect of Reynolds number variation at fixed *Re*.

ACKNOWLEDGMENT

The authors thank to the King Abdullah University of Science and Technology (KAUST), Supercomputing Laboratory, and HPC Resources (KAUST), for providing computing resources.

REFERENCES

[1] R. Shrestha, M. Benedict, V. Hrishikeshavan, and I. Chopra, "Hover performance of a small-scale helicopter rotor for flying on Mars," *J. Aircr.*, vol. 53, no. 4, pp. 1160–1167, Jul. 2016.

[2] J. Liu, D. Li, Z. Zuo, C. Liu, and H. Wang, "Aerodynamic performance of a characteristic airfoil at low-Reynolds number and transonic flow under Mars sand-containing environment," *Phys. Fluids*, vol. 35, no. 76120, pp. 1–16, Jul. 2023.

[3] J. Xu, D. Li, W. Song, Z. Han, and H. Li, "Design optimization of airfoils at ultra-low Reynolds numbers," in *Proc. 32nd Congr. Int. Council Aeronaut. Sci. (ICAS)*, Shahnghai, China, 2021, pp. 1–12.

[4] J. Winslow, H. Otsuka, B. Govindarajan, and I. Chopra, "Basic understanding of airfoil characteristics at low Reynolds numbers (10 4–10 5)," *J. Aircr.*, vol. 55, no. 3, pp. 1050–1061, 2018.

[5] O. Günel, E. Koç, and T. Yavuz, "CFD vs. XFOIL of airfoil analysis at low Reynolds numbers," in *Proc. IEEE Int. Conf. Renew. Energy Res. Appl. (ICRERA)*, Nov. 2016, pp. 628–632.

[6] N. Naeem, M. Güney, and M. Fouda, "Wake patterns and mode switching at low Reynolds numbers," *Prog. Comput. Fluid Dyn., Int. J.*, vol. 23, no. 2, p. 87, 2023.

[7] D. F. Kurtulus, "Vortex flow aerodynamics behind a symmetric airfoil at low angles of attack and Reynolds numbers," *Int. J. Micro Air Vehicles*, vol. 13, Jan. 2021, Art. no. 175682932110556.

[8] T. Kouser, Y. Xiong, D. Yang, and S. Peng, "Numerical study on drag reduction and wake modification for the flows over a hydrofoil in presence of surface heterogeneity," *Adv. Mech. Eng.*, vol. 14, no. 1, Jan. 2022, Art. no. 168781402210753.

[9] D. Mateescu and M. Abdo, "Analysis of flows past airfoils at very low Reynolds numbers," *Proc. Inst. Mech. Eng., G, J. Aerosp. Eng.*, vol. 224, no. 7, pp. 757–775, Jul. 2010.

[10] R. T. Islam, M. Z. Alam, D. Ali, and M. Taher, "Experimental study of aerodynamic co-efficients, co-efficient of pressure and flow-field around NACA 0012 airfoil," Tech. Rep., 2023, vol. 12.

[11] H. Tang, Y. Lei, X. Li, K. Gao, and Y. Li, "Aerodynamic shape optimization of a wavy airfoil for ultra-low Reynolds number regime in gliding flight," *Energies*, vol. 13, no. 2, p. 467, Jan. 2020.

[12] D. Antonelli, C. Sacco, and J. Tamagno, "Flow simulations with ultra-low Reynolds numbers over rigid and flexible airfoils subject to heaving and flapping motions," *J. Appl. Fluid Mech.*, vol. 10, no. 2, pp. 749–762, Mar. 2017.

[13] M. G. Ukken and M. Sivapragasam, "Aerodynamic shape optimization of airfoils at ultra-low Reynolds numbers," *Sādhanā*, vol. 44, no. 6, p. 130, Jun. 2019.

[14] D. F. Kurtulus, "Unsteady aerodynamics of a pitching NACA 0012 airfoil at low Reynolds number," *Int. J. Micro Air Vehicles*, vol. 11, Jan. 2019, Art. no. 175682931989060.

[15] T. Kouser, Y. Xiong, D. Yang, and S. Peng, "Direct numerical simulations on the three-dimensional wake transition of flows over NACA0012 airfoil at Re= 1000," *Int. J. Micro Air Vehicles*, vol. 13, Nov. 1000, Art. no. 17568293211055656.

[16] E. Uddin, M. A. Naseem, S. U. Khalid, A. Mubashar, and S. R. Shah, "Investigation of the flow around uncambered airfoils at 1000 Reynolds number using computational fluid dynamics for micro air vehicles," in *Proc. World Congr. Adv. Structural Eng. Mech.*, 2017.

[17] C. Huang, L. Zhao, J. P. Niu, J. J. Di, J. J. Yuan, Q. L. Zhao, F. Q. Zhang, Z. H. Zhang, J. M. Lei, and G. P. He, "Coupled particle and mesh method in an Euler frame for unsteady flows around the pitching airfoil," *Eng. Anal. Boundary Elements*, vol. 138, pp. 159–176, May 2022.

[18] T. Bao, J. Hu, C. Huang, and Y. Yu, "Smoothed particle hydrodynamics with κ-ε closure for simulating wall-bounded turbulent flows at medium and high Reynolds numbers," *Phys. Fluids*, vol. 35, no. 8, 2023, Art. no. 085114.

[19] T. H. Pulliam and J. A. Vastano, "Transition to chaos in an open unforced 2D flow," *J. Comput. Phys.*, vol. 105, no. 1, pp. 133–149, Mar. 1993.

[20] D. Durante, E. Rossi, and A. Colagrossi, "Bifurcations and chaos transition of the flow over an airfoil at low Reynolds number varying the angle of attack," *Commun. Nonlinear Sci. Numer. Simul.*, vol. 89, Oct. 2020, Art. no. 105285.

[21] J. Chang, Q. Zhang, L. He, and Y. Zhou, "Shedding vortex characteristics analysis of NACA 0012 airfoil at low Reynolds numbers," *Energy Rep.*, vol. 8, pp. 156–174, Jul. 2022.

[22] E. Rossi, A. Colagrossi, G. Oger, and D. Le Touzé, "Multiple bifurcations of the flow over stalled airfoils when changing the Reynolds number," *J. Fluid Mech.*, vol. 846, pp. 356–391, Jul. 2018.

[23] Y. Elimelech, R. Arieli, and G. Iosilevskii, "Flow over NACA-0009 and eppler-61 airfoils at Reynolds numbers 5000 and 60,000," *AIAA J.*, vol. 45, no. 10, pp. 2414–2421, Oct. 2007.

[24] J. Deng, L. Sun, and X. Shao, "Wake dynamics of low-Reynolds-number flow around a two-dimensional airfoil," *Phys. Fluids*, vol. 31, no. 2, Feb. 2019, Art. no. 024102.

[25] M. Gopalakrishnan Meena, K. Taira, and K. Asai, "Low Reynolds number wake modification using a gurney flap," in *Proc. 55th AIAA Aerosp. Sci. Meeting*, Jan. 2017, p. 0543.

[26] D. F. Kurtulus, "On the wake pattern of symmetric airfoils for different incidence angles at Re = 1000," *Int. J. Micro Air Vehicles*, vol. 8, no. 2, pp. 109–139, Jun. 2016.

[27] P. A. C. Rocha, H. H. B. Rocha, F. O. M. Carneiro, M. E. V. da Silva, and C. F. de Andrade, "A case study on the calibration of the k–ω SST (shear stress transport) turbulence model for small scale wind turbines designed with cambered and symmetrical airfoils," *Energy*, vol. 97, pp. 144–150, Feb. 2016.

[28] S. A. Khan, M. Bashir, M. A. Ali Baig, and F. A. Ghasi Mehaboob Ali, "Comparing the effect of different turbulence models on the CFD predictions of NACA0018 airfoil aerodynamics," *CFD Lett.*, vol. 12, no. 3, pp. 1–10, Mar. 2020.

[29] R. B. Langtry and F. R. Menter, "Correlation-based transition modeling for unstructured parallelized computational fluid dynamics codes," *AIAA J.*, vol. 47, no. 12, pp. 2894–2906, Dec. 2009.

[30] D. Kurtulus, "Critical angle and fundamental frequency of symmetric airfoils at low Reynolds numbers," *J. Appl. Fluid Mech.*, vol. 15, no. 3, 2022.

[31] S. Sunada, A. Sakaguchi, and K. Kawachi, "Airfoil section characteristics at a low Reynolds number," *J. Fluids Eng.*, vol. 119, no. 1, pp. 129–135, Mar. 1997.

[32] D. J. Cleaver, Z. Wang, and I. Gursul, "Bifurcating flows of plunging aerofoils at high strouhal numbers," *J. Fluid Mech.*, vol. 708, pp. 349–376, Oct. 2012.

[33] S. Gupta, J. Zhao, A. Sharma, A. Agrawal, K. Hourigan, and M. C. Thompson, "Two-and three-dimensional wake transitions of a NACA0012 airfoil," *J. Fluid Mech.*, vol. 954, p. A26, Aug. 2023.

[34] M. Abdo and D. Mateescu, "Low-Reynolds number aerodynamics of airfoils at incidence," in *Proc. 43rd AIAA Aerosp. Sci. Meeting Exhib.*, Jan. 2005, p. 1038.

[35] P. J. Kunz, "Analysis and design of airfoils for use at ultra-low Reynolds numbers," in *Fixed and Flapping Wing Aerodynamics for Micro Air Vehicle Applications*. American Institute of Aeronautics and Astronautics, 2001.

[36] D. F. Kurtulus, "On the unsteady behavior of the flow around NACA 0012 airfoil with steady external conditions at Re=1000," *Int. J. Micro Air Vehicles*, vol. 7, no. 3, pp. 301–326, Sep. 2015.

[37] C. Pranesh, M. Sivapragasam, and M. D. Deshpande, "Aerodynamic characteristics of flow past NACA 0008 airfoil at very low Reynolds numbers," *J. Aerosp. Sci. Technol.*, vol. 66, pp. 247–266, Aug. 2023.

[38] K. Menon and R. Mittal, "Aerodynamic characteristics of canonical airfoils at low Reynolds numbers," *AIAA J.*, vol. 58, no. 2, pp. 977–980, Feb. 2020.

[39] C. H. K. Williamson and A. Roshko, "Vortex formation in the wake of an oscillating cylinder," *J. Fluids Struct.*, vol. 2, no. 4, pp. 355–381, Jul. 1988.

[40] A. Aravind, P. Kumar Seshadri, and A. De, "Leading edge vortex dynamics of airfoils, pitching continuously at high amplitudes," 2021, *arXiv:2108.06275*.

[41] S. J. Schreck, W. E. Faller, and M. C. Robinson, "Unsteady separation processes and leading edge vortex precursors: Pitch rate and Reynolds number influences," *J. Aircr.*, vol. 39, no. 5, pp. 868–875, Sep. 2002.
[42] S. N. Pillai, A. Sundaresan, R. Gopal, S. B. M. Priya, A. A. Pasha, A. Z. Hameed, A. G. A. Jameel, V. M. Reddy, and K. A. Juhany, "Estimation of chaotic surface pressure characteristics of ice accreted airfoils—A 0–1 test approach," *IEEE Access*, vol. 9, pp. 114441–114456, 2021.
[43] X. Qin, P. Liu, and Q. Qu, "Aerodynamics of a multi-element airfoil near ground," *Tsinghua Sci. Technol.*, vol. 14, no. S2, pp. 94–99, Dec. 2009.
[44] O. Marquet, J. S. Leontini, J. Zhao, and M. C. Thompson, "Hysteresis of two-dimensional flows around a NACA0012 airfoil at Re=5000 and linear analyses of their mean flow," *Int. J. Heat Fluid Flow*, vol. 94, Apr. 2022, Art. no. 108920.
[45] S. Wang, Y. Zhou, M. M. Alam, and H. Yang, "Turbulent intensity and Reynolds number effects on an airfoil at low Reynolds numbers," *Phys. Fluids*, vol. 26, no. 11, pp. 1–9, Nov. 2014.
[46] S. Mittal and T. Tezduyar, "Massively parallel finite element computation incompressible flows involving fluid-body interactions," *Appl. Mech. Eng.*, vol. 108, pp. 99–118, Jun. 1993.
[47] M. M. Alam, Y. Zhou, H. X. Yang, H. Guo, and J. Mi, "The ultra-low Reynolds number airfoil wake," *Experim. Fluids*, vol. 48, no. 1, pp. 81–103, Jan. 2010.

TAIBA KOUSER was born in Faisalabad, Pakistan. She received the Ph.D. degree from the School of Aerospace Engineering, Huazhong University of Science and Technology, Wuhan, China, in 2021. Currently, she is a Postdoctoral Researcher with the Applied Research Center for Metrology, Standards, and Testing (ARC-MST), King Fahd University of Petroleum and Minerals (KFUPM), Dhahran, Saudi Arabia. Her research interests include computational fluid dynamics, drag reduction, and unsteady aerodynamics and aeroacoustics.

DILEK FUNDA KURTULUS received the B.S. and M.S. degrees in aerospace engineering from Middle East Technical University, Ankara, Turkey, in 2000 and 2002, respectively, and the Ph.D. degree in aerospace engineering from ENSMA/Université de Poitiers, Poitiers, France. In 2006, she was Postdoctoral Researcher with Laboratoire d'Etudes Aérodynamique, ENSMA Poitiers, and the Laboratoire de Combustion et Systèmes Réactifs, CNRS, Orléans, France. Since 2018, she has been a Professor with the Department of Aerospace Engineering, Middle East Technical University. Her research interests include aircraft design, unsteady aerodynamics, and unmanned air vehicles. She was a recipient of the Amelia Earhart Fellow at Zonta International, in 2005, the NATO Scientific Achievement Award, in 2011, the Turkish Academy of Science Young Scientific Award, in 2012, and the Zonta International Centennial Recognition Award of Turkey, in 2019.

ABDULRAHMAN ALIYU received the B.Eng. degree in electrical engineering from Bayero University, Kano, Nigeria, in 2010, and the M.S. and Ph.D. degrees in systems and control engineering from the King Fahd University of Petroleum and Minerals, in 2016 and 2020, respectively. He is currently a Postdoctoral Fellow with the Applied Research Center for Metrology, Standards and Testing, King Fahd University of Petroleum and Minerals. His research interests include robotics, control theory, multi-agent/large-scale systems, artificial intelligence, energy harvesting, metrology, and sensors.

SRIKANTH GOLI was born in Hyderabad, India. He received the B.Tech. degree in aeronautical engineering from Jawaharlal Nehru Technological University, in 2008, the M.E. degree in aeronautical engineering from the Hindustan Institute of Technology and Science, in 2011, and the Ph.D. degree from the Department of Aerospace Engineering, IIT Kharagpur, India, in 2019. From 2019 to 2022, he carried out research at various academic institutions and industries. He is currently a Postdoctoral Researcher with the Applied Research Center for Metrology, Standards, and Testing (ARC-MST), King Fahd University of Petroleum and Minerals (KFUPM), Saudi Arabia. His research interests include aircraft design, experimental and numerical fluid dynamics, and unmanned air vehicles. He has memberships in professional societies, such as the National Society of Fluid Mechanics and Fluid Power, the Indian Society of Theoretical and Applied Mechanics, and the Aeronautical Society of India.

LUAI M. ALHEMS received the Ph.D. degree from Texas A&M University, College Station, TX, USA, in 2002. He is currently a Professor of thermo-fluid with the Department of Mechanical Engineering, King Fahd University of Petroleum and Minerals (KFUPM), Dhahran, Saudi Arabia. He is also the Director of the Applied Research Center for Metrology, Standards, and Testing (ARC-MST) Research Institute. Regional authorities have recognized him for his research work. He has authored or coauthored more than 180 journal articles and patents. His research interests include gas turbines, energy systems, failure analysis, wind energy, and energy conservation.

IMIL HAMDA IMRAN received the B.S. degree in electrical engineering from Andalas University, Indonesia, in 2011, the M.S. degree in systems and control engineering from the King Fahd University of Petroleum and Minerals, Saudi Arabia, in 2015, and the Ph.D. degree in electrical engineering from The University of Newcastle, Australia, in 2020. He was a Postdoctoral Research Associate with the Department of Engineering, Lancaster University, U.K., in 2022. He is currently a Postdoctoral Fellow with the Applied Research Center for Metrology, Standards, and Testing, King Fahd University of Petroleum and Minerals. His research interests include networked control systems, multi-agent systems, nonlinear control, and adaptive control.

AZHAR M. MEMON was born in Pakistan, in 1987. He received the B.E. degree in electronics from the National University of Sciences and Technology (NUST), Pakistan, in 2009, the M.Sc. degree in automation and control engineering from the National University of Singapore (NUS), Singapore, in 2010, and the Ph.D. degree from the King Fahd University of Petroleum and Minerals (KFUPM), Saudi Arabia, in 2015. From 2009 to 2010, he was a Research Engineer with NUS and a Lecturer in 2011. He joined the Research and Development Department, Rosen Group, as a Sensors and Algorithm Specialist. In 2019, he joined KFUPM as an Assistant Professor, where he is actively participating in managing various client-funded and internally-funded research projects and teaching. He has authored or coauthored several peer-reviewed research articles and conference papers in reputable journals and international conferences. His research interests include control systems, signal processing, data analytics, nondestructive testing, and aquaponics. For more information please visit www.azharmemon.com.